Premelting Dynamics

J.S. Wettlaufer[1] and M. Grae Worster[2]

[1] Department of Geology and Geophysics, Department of Physics, Yale University, New Haven, Connecticut 06520-8109; email: john.wettlaufer@yale.edu

[2] Institute of Theoretical Geophysics, Department of Applied Mathematics and Theoretical Physics, Centre for Mathematical Sciences, University of Cambridge, Cambridge CB3 0WA, United Kingdom; email: grae@damtp.cam.ac.uk

Key Words

thin films, frost heave, interfaces, phase changes, solidification

Abstract

When the free surfaces of most solids approach their bulk melting temperatures from below, the molecular structure of the material gives way to a disordered structure with some attributes of both the solid and liquid phases. When the temperature is sufficiently close to that of bulk transition, the surface melts and literally flows as a viscous fluid. This phenomenon, called interfacial premelting, lies at the heart of the microscopic theory of melting of solid matter, and captures the interest of condensed matter physicists and physical chemists alike. The process is ubiquitous and responsible for a wide range of consequences in materials with biological, geophysical, and technological significance. Because such systems are often exposed to spatial or temporal variations in thermodynamic forcing, there are a host of fluid mechanical phenomena that result from this underlying melting behavior. The fluid dynamics of unfrozen surfaces holds clues for understanding the bulk behavior of polycrystalline materials, from Earth's mantle to the stratosphere and beyond. In this review we focus on the fluid dynamical consequences of the premelting of solids.

1. INTRODUCTION

The surface of a material is a place where two and three dimensions meet and the microscopic structure of one phase must make compromises with that of another. The physics of the surface and that of the bulk are most often taught and studied in isolation, but the confluence of dimensionality and phase behavior found at the surface provides a wide-ranging area of exploration in physical, chemical, and biological science. There are two intrinsic aspects of surfaces that are familiar to those working in fluid mechanics: wetting phenomena and thermophoretic (Marangoni) flows. In the simplest case of wetting, the force balance that determines the necessary conditions for the spreading of a liquid droplet on a chemically inert substrate involves the contact line where the substrate, the wetting liquid, and the surrounding phase come together. The leading-order force balance involves the relevant surface energies (tensions in the case of a fluid), and a more careful description brings in long-ranged intermolecular interactions, such as van-der-Waals forces, that underlie the surface energy. During thermophoresis, for example, the temperature dependence of the surface tension between two immiscible fluids drives fluid flow. Similarly, in a two-component fluid, such as many alcohols, the surface tension depends on composition, and hence the volatility of one species can give rise to gradients in surface tension that induce flows: "legs" or "tears" of wine are a common example (e.g., deGennes et al. 2004). The topic of this review makes some contact with these phenomena but is quite distinct in its origin and consequences: Flow of interfacially premelted fluid would not occur in the absence of interfaces, but its existence requires neither contact lines nor gradients in the coefficients of surface energy. The topic occupies a curious interfacial position between condensed matter physics and fluid mechanics.

The effects of composition on the phase of a material are familiar: Those living in cold climates know that roads are salted to melt ice. The origin of the freezing-point depression in solutions is the same as the origin of osmotic pressure: the reduction in the chemical potential of the solvent in the presence of the solute. The effect is to shift the equilibrium domain of the liquid phase into the solid region of the bulk-phase diagram in the absence of solute; that is, the freezing point is depressed by the addition of solute. Other effects also extend the equilibrium domain of the liquid phase into solid territory. For example, it is well known that a small convex solid particle is in metastable equilibrium with its supercooled melt. This so-called Gibbs-Thomson effect is due to the competition between the reduction in the bulk free energy upon formation of the solid phase and the increase in free energy associated with the required formation of the surface. This competition is responsible for this hallmark of nucleation: An incipient crystal must reach a certain critical size before it can grow into a supercooled melt (e.g., Davis 2001; Oxtoby 2002, 2003). More broadly, the Gibbs-Thomson effect has profound implications for the phase behavior of polycrystals, and has a long history of study in a wide range of materials (e.g., Cahn 1991, Smith & Guttman 1953).[1] The inability, conversely, to superheat solids has a different technical origin, but we can think of it in similar thermodynamic terms.

---

[1]We refer the reader with interests in metallurgy to these papers and references therein.

It originates in the process responsible for the nature of melting, which also alters the equilibrium states of matter near interfaces; although a material below its bulk freezing temperature is solid in the main, it can be liquid in a thin layer adjacent to another bulk phase in thermodynamic equilibrium. This forms the basic topic of our fluid mechanical investigations.

## 2. MELTING AND PREMELTING: BACKGROUND AND EVIDENCE

After nearly a century-long search for a microscopic theory of melting, it is now understood that the basic process, as it occurs in virtually every solid, originates at its boundaries (Dash 2002). The details depend on the structure of, and intermolecular interactions across, the bounding materials. Generally speaking, we reserve the term surface melting for the process as it occurs at the vapor interface, interfacial melting when melting takes place against a foreign substrate, and grain-boundary melting when considering the interface between two crystallites of the same substance. Together they are referred to as interfacial premelting, and together with compositional and Gibbs-Thomson effects they complete the list of premelting phenomena. The process of surface or interfacial premelting begins at a temperature below the bulk melting point T_m as a molecularly thin liquid-like film. When the melting is complete, the film thickness increases with temperature and becomes macroscopically thick when the bulk melting temperature is reached. Conversely, where retarded potential effects intervene and attenuate the intermolecular wetting forces, the film growth may be blocked and the film may thereby be finite at the bulk transition. This circumstance is referred to as incomplete melting (e.g., Benatov & Wettlaufer 2004, Elbaum & Schick 1991, Wilen et al. 1995).

Surface melting has been observed in low-vapor-pressure systems with molecular-scale precision because of the ability to exploit many of the structurally specific methods of surface science. The surface and interfacial melting of metals, solid rare gases, quantum solids, semiconductors, and molecular solids have been confirmed using a variety of experimental methods. The approaches range from scattering of atoms or bright X rays, which probe atomic or molecular-scale disorder, to interference of visible light, which distinguishes between solid and liquid (see reviews by Dash et al. 1995, 2006). The different approaches are important conceptually because they probe different structural aspects of the route to melting. They are also important practically because for a high-vapor-pressure material such as ice, standard surface-science methodology is compromised by interactions with the vapor phase. During interfacial melting, the roughness of the wall can influence the process in a manner similar to the role of corrugations in wetting (Bednorz & Napiorkowski 2000, Netz & Andelman 1997, Rascon & Parry 2000). In short, mobile liquid is observed sufficiently close to the bulk melting temperature on at least one facet of this wide class of materials. However, to clarify the connections to, and the distinctions from, phenomena more familiar to the fluid mechanics community, we begin by briefly summarizing the observations of premelted liquid water at ice surfaces, which is our main focus.

Ice exhibits all aspects of premelting, and the implications include, among other things, the ozone-destroying heterogeneous chemistry on polar stratospheric cloud particles, the electrification of thunderclouds, the trapping and redistribution of climate proxies in ice sheets, the mechanics of temperate glaciers, and frost heave in partially frozen soils. For these and other reasons, the premelting of ice has been examined in many laboratory studies. There are several recent reviews of the condensed matter physics and physical chemistry of interfacial premelting with a particular emphasis on ice (Dash et al. 1995, 2006; Ewing 2004; Girardet & Toubin 2001). Although there is variability among laboratories, due in part to the origins of surface sensitivity and the high vapor pressure, progress has been made using a variety of methods (Barer et al. 1977, Beaglehole & Nason 1980, Beaglehole & Wilson 1994, Bluhm et al. 2002, Dosch et al. 1995, Eastman & Zhu 1995, Elbaum et al. 1993, Engemann et al. 2004, Ewing 2004, Furukawa et al. 1987, Ishizaki et al. 1996, Pittenger et al. 2001, Sadtchenko & Ewing 2002, Wilen & Dash 1995).[2] For reference, the interfacially premelted film separating ice from a planar substrate is typically of order 10^{-8} m thick when the temperature is a few tenths of a degree below the bulk melting temperature (e.g., Sadtchenko & Ewing 2002). Understanding grain-boundary melting is important because of its central influence on sintering and coarsening in all materials. However, direct observation of grain-boundary melting is a serious experimental challenge because of the difficulty of accessing the interface in thermodynamic equilibrium. Computer simulations and theory support the notion of disorder at a grain boundary (e.g., Broughton & Gilmer 1986, Kikuchi & Cahn 1980, Schick & Shih 1987), but the role of impurities is particularly important in the case of ice because of the high solubility of electrolytes in water (Benatov & Wettlaufer 2004, Ewing 2004, Wettlaufer 1999).

At temperatures near T_m, polycrystalline ice contains liquid water due mainly to the impurity and curvature depressions of the freezing point (e.g., Mader 1992a,b; Nye 1992). The unfrozen water is found in microscopic channels (10–100 μm) called veins where three grains abut and at nodes separating four grains (**Figure 1**). Hence, due solely to curvature and impurity effects, the equilibrium structure of polycrystalline ice is characterized by a connected network of water. We emphasize here that the detailed quantitative effects of impurities and phase-boundary curvature depend on system specificity and in particular whether solutes appear in a surface-melted film or in a bulk fluid. This is well documented for ice (e.g., Boxe et al. 2003; Campen et al. 2003; Cho et al. 2002; Doppenschmidt & Butt 2000; Girardet & Toubin 2001; Huthwelker et al. 2001; Khvorostyanov & Curry 2004; Mader 1992a,b; Nye 1991; Rempel et al. 2001b; Rempel & Wettlaufer 2003a; Tsionsky et al. 2002; Warren & Hudson 2003). The implications can be dramatic. For example, Rempel et al. (2001b) and Rempel & Wettlaufer (2003a,b) found that diffusion of soluble impurities coupled with phase change through this premelted network can, over long time periods, lead to significant effects in the redistribution of climate proxies in ice sheets, but these effects are not discussed here.

---

[2] We note that despite lower spatial resolution, optical methods have the advantage of unambiguously defining the bulk liquid phase.
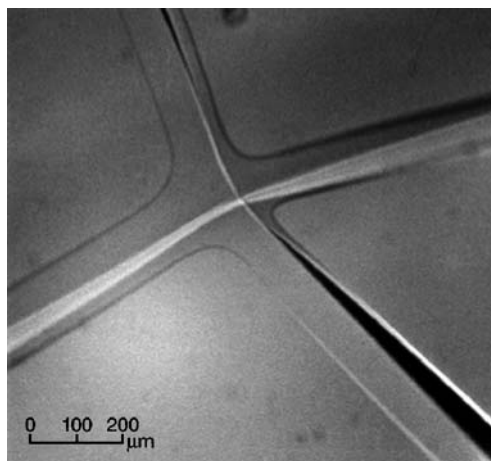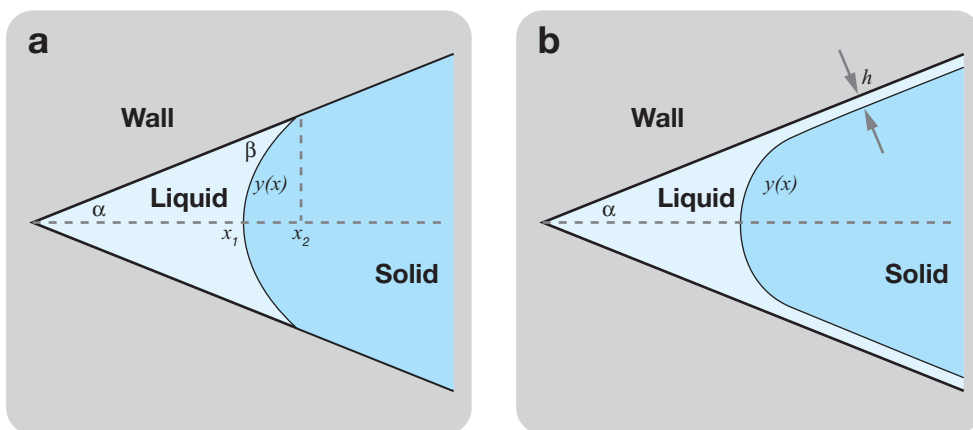
Figure 1

Photograph of four veins intersecting at a node between four crystals of ice near, but below, 0°C. Photo taken by H. Mader, University of Bristol. This three-dimensional network of veins and nodes characterizes the continuous liquid network of polycrystalline ice below the bulk melting temperature.

Nye & Frank (1973) predicted the geometry of the network shown in **Figure 1** under the assumption that the interfacial energies are independent of crystallographic orientation, and Rempel (2000) used similar ideas to determine the equilibrium geometry of ice confined in a wedge bounded by chemically inert material. Their results are analogous to the determination of the contact angle of a nonwetting fluid on a substrate (deGennes 1985), and these ideas, which are familiar from other fluid mechanical contexts, form the starting point for our detailed examination of premelting in the next section.

3. PHASE EQUILIBRIUM IN CONFINED SYSTEMS

We are concerned with the behavior of materials at temperatures close to their bulk melting temperature T_m when they are confined, for example within the interstices of a porous rock, by a surrounding medium, such as the case of an ice crystal in air, or by other grains of similar material. We shall see that the phase of the material, whether it is solid or liquid, is determined in part by its proximity to the confining boundary. In particular, many confined solids become liquid close to the boundary. In a pure system, this liquid can flow either in response to an externally applied pressure gradient or in response to an applied temperature gradient. It is the latter type of flow, which is peculiar to the thermodynamic interactions occurring near interfaces between adjacent materials, that forms the focus of this article.

We begin by describing the thermodynamics of confined materials. Much of this is analogous to the problem of wetting in wedges (e.g., Bednorz & Napiorkowski 2000, Netz & Andelman 1997, Rascon & Parry 2000), but there are important differences. As a canonical example, consider a material at uniform temperature $T < T_m$

Figure 2

Schematic of the intrusion of the solid phase into a wedge-shaped substratum. In (*a*) the contact angle β is finite and in (*b*) it is zero, indicating that there is interfacial premelting between the solid phase and the substratum. The phase behavior near the apex is dominated by the Gibbs-Thomson effect.

confined within a two-dimensional wedge of half-angle α, as shown in **Figure 2**. The melting temperature of a convex solid is depressed, as we see in detail below, so the possibility arises that the solid phase does not extend into the apex of the wedge. In general, therefore, there will be interfaces separating each of the solid and liquid phases from the confining wall as well as an interface separating the solid and liquid phases of the confined material. The latter is always a free boundary that adjusts to the prevailing thermodynamic conditions. **Figure 2a** shows a state in which the solid-liquid interface intersects the boundary of the wedge at some contact angle β. The shape and position of the solid–liquid phase boundary, including the contact angle, can be determined by minimizing the total free energy of the system as follows.

There is a surface energy per unit area associated with each of the interfaces: γ_{sl}, γ_{lw}, and γ_{sw} for the solid-liquid, liquid-wall, and solid-wall interfaces, respectively. Therefore, the Helmholtz free energy of the state depicted in **Figure 2**, relative to a state in which solid fills the wedge completely, is

$$F = (p_s - p_l)\left[\frac{1}{2}x_2^2 \tan \alpha - \int_{x_1}^{x_2} y\,dx\right] + (\gamma_{lw} - \gamma_{sw})x_2 \sec \alpha + \gamma_{sl}\int_{x_1}^{x_2} \sqrt{1 + y'^2}\,dx,$$

$$(3.1)$$

where p_s and p_l are the pressures in the solid and liquid phases, respectively, and we assume that the system is symmetric about the center of the wedge. The equilibrium shape of the solid-liquid interface $y(x)$ is determined by minimizing F with respect to variations in y leading to Euler-Lagrange equations. This shows, straightforwardly, that the interface is circular with radius of curvature

$$R = \frac{\gamma_{sl}}{p_s - p_l}. \qquad (3.2)$$

The Gibbs-Duhem relationship for phase equilibrium (Reif 1965) states, quite generally, that

$$p_s - p_l = \rho_s \mathcal{L} \frac{T_m - T}{T_m} - (p_l - p_m)\left(1 - \frac{\rho_s}{\rho_l}\right), \tag{3.3}$$

where $\mathcal{L}$ is the latent heat of fusion and p_m is the reference pressure at which the bulk melting temperature of the solid is equal to T_m. Combining this with Equation 3.2 shows that

$$\rho_s \mathcal{L} \frac{T_m - T}{T_m} = (p_l - p_m)\left(1 - \frac{\rho_s}{\rho_l}\right) + \frac{\gamma_{sl}}{R}. \tag{3.4}$$

The first term on the right-hand side describes pressure melting, whereby ice (for which $\rho_s < \rho_l$) has a lower melting temperature at higher pressures, whereas the second term gives rise to the Gibbs-Thomson relationship that convex solids have lower melting temperatures the higher the curvature of their bounding interface. In this article, we ignore pressure melting by setting $\rho_s = \rho_l$. However, we note that this is simply dealt with by properly accounting for the dependence of T_m on pressure through the Clausius-Clapeyron slope. Because the magnitude of this effect is negligible (see, e.g., Equation 2.7 of Dash et al. 1995), it does not play a significant role in premelting dynamics.

Although liquids can exist in a metastable supercooled state, a consequence of premelting (derived below) is that solids cannot similarly be superheated. That is, their temperature must always be below their (pressure-dependent) bulk melting temperature. This in turn means that $p_s - p_l$ must be positive, which can be shown using Equation 3.3, and hence R must also be positive when the center of curvature is in the solid. This distinguishes the present situation from the apparently similar situation in which the region of solid in **Figure 2a** is replaced by another fluid. In the latter case, the surface energy can be interpreted as a surface tension with mechanical equilibrium holding the interface circular, and Equation 3.2 holds with the possibility of R having either sign.

The minimum value of the free energy can now be determined geometrically to be

$$F = (p_s - p_l)\frac{R^2}{2}\left[\frac{\cos\beta\,\cos(\alpha+\beta)}{\sin\alpha - \left(\frac{\pi}{2} - \alpha - \beta\right)}\right] + (\gamma_{lw} - \gamma_{sw})R\frac{\cos(\alpha+\beta)}{\sin\alpha - \gamma_{sl}R\left(\frac{\pi}{2} - \alpha - \beta\right)}. \tag{3.5}$$

This expression can be minimized with respect to the contact angle β to show, in conjunction with Equation 3.2, that

$$\cos\beta = \frac{\gamma_{sw} - \gamma_{lw}}{\gamma_{sl}}. \tag{3.6}$$

The Young-Dupré equation (Equation 3.6) is often derived as a force balance in the plane of the wall at the contact line where the three phases meet. However, the a priori assumption of mechanical equilibrium seems inappropriate when, as here, one or more of the phases is a solid that can support elastic stresses, not accounted for in the force balance. Additionally, whereas the equilibrium state can be approached by material transport when at least two of the phases are fluid, in the present case

equilibrium is approached by phase change (solidification or melting) without requiring any material transport. This is an important realization indicating that the solid-liquid interface, which will form at least one boundary of all the fluid flows we shall consider, although a free boundary, is determined thermodynamically and not directly by fluid transport, as would be the case for a liquid-vapor interface, for example. Nevertheless, we shall see that there are important interactions between fluid mechanics and thermodynamics that ultimately determine the position of the phase boundary and the overall dynamics of the system.

The topology represented in **Figure 2a** is only possible if $\Delta\gamma \equiv \gamma_{sl} + \gamma_{lw} - \gamma_{sw} > 0$ (since $\cos\beta < 1$), and Equation 3.6 shows further that the contact angle tends to zero as $\Delta\gamma$ tends to zero.

If $\Delta\gamma$ is negative then the energy of the solid-wall interface is reduced when there is an intermediate layer of liquid, as shown in **Figure 2b**. The generation of such a liquid film is an example of interfacial premelting. A detailed analysis of this situation is given by Rempel (2000), who showed that the solid is separated from the wall by a thin, uniform layer of liquid, of thickness h say, far from the apex and that the solid-liquid interface has almost uniform curvature, given by Equation 3.2, until it reaches a distance of order h from the wall. Typically $h/R \ll 1$.

An expression for the thickness h of the interfacially premelted liquid film far from the apex of the wedge can be obtained by considering, for example, the influence of the dispersion forces acting across it on its chemical potential. We describe the thermodynamics of surface and interfacial premelting first by analogy with a very familiar circumstance. In the absence of an external field, a body in thermodynamic equilibrium has a constant temperature T, pressure p, and chemical potential μ. However, in the presence of an external field, the condition for equilibrium is constancy of temperature and chemical potential of the body, the latter being modified by the field energy per molecule. Hence, in a uniform gravitational field, for example, in which the potential energy of a molecule $U(z) = mgz$ is solely a function of the vertical coordinate z of its center of mass, its molecular mass m, and the gravitational acceleration g, the condition for equilibrium of an isothermal body is

$$\mu(T, p, z) = \mu_0(T, p) + U(z) = constant, \tag{3.7}$$

where $\mu_0(T, p)$ is the chemical potential of the body in the absence of the gravitational field. For a body of constant density, the intensivity of chemical potential as embodied in Equation 3.7 leads to the usual formula for hydrostatic equilibrium of an incompressible body, namely because

$$d\mu(T, p, z) = \left[\frac{\partial\mu(T, p, z)}{\partial p}\right]_{T,z} dp + \left[\frac{\partial\mu(T, p, z)}{\partial z}\right]_{p,T} dz = 0, \tag{3.8}$$

and the molecular volume is $v \equiv [\partial\mu/\partial p]_{T,z}$, we find $dp = mv^{-1}gdz \equiv -\rho_o gdz$. Fluid dynamicists may be more familiar with the idea that force balances lead to the hydrostatic equation, and yet we see here that the relation can be derived from the general considerations of the shift in equilibrium thermodynamic states associated with an external field energy per molecule. It is a generic result that the introduction

of such a field is responsible for the introduction of a new pair of canonically conjugate thermodynamic variables.

The thermodynamic equilibrium between a solid (s) and a liquid (l) is characterized by the intensivity of chemical potential, which requires that $\mu_s(T, p) = \mu_l(T, p)$ for the locus of temperatures and pressures along coexistence. Hence, by definition, departures from coexistence enter into the bulk region of either phase by varying the temperature or pressure or both:

$$\mu_s(T, p) - \mu_l(T, p) \equiv \Delta\mu \approx \left[\frac{\partial \Delta\mu}{\partial T}\right]_{T_m, p_m} (T - T_m) + \left[\frac{\partial \Delta\mu}{\partial p}\right]_{T_m, p_m} (p - p_m) + \text{h.o.t.}$$
(3.9)

For interfacial premelting, long-ranged intermolecular interactions provide the field energy per molecule that shifts the equilibrium domain of the liquid phase into the solid region of the bulk-phase diagram and hence $\Delta\mu > 0$. Thus, for an interfacial film of thickness h, the expression analogous to Equation 3.7, but here for the chemical potential of the film, is

$$\mu_f(T, p, h) = \mu_l(T, p) + U'(h) = \mu_s(T, p),$$
(3.10)

where $U'(h)$ is the derivative, with respect to h, of the underlying effective interfacial free energy $U(h)$, which itself depends on the nature of the intermolecular interactions in the system (e.g., Dash 2002, Dash et al. 1995, deGennes 1985, Dietrich 1988, Lipowsky 1982, Schick 1990). Hence, for example, in the case of nonretarded vander-Waals forces, a phenomenological description is given by

$$U'(h) = \frac{2\Delta\gamma\sigma^2}{\rho_l h^3},$$
(3.11)

where σ is of order a molecular length, ρ_l is the liquid density, and $\Delta\gamma \equiv \gamma_{sl} + \gamma_{lw} - \gamma_{sw}$ is the difference between the interfacial energy of the dry interface between the solid (s) phase and the third phase (w), be it the vapor, a chemically inert wall, or a different orientation of the solid phase. It can be shown (Wettlaufer & Worster 1995) that the coefficient in Equation 3.11 is related to the Hamaker constant $\mathcal{A}$ and the spreading parameter $\mathcal{S}$ by $\mathcal{A}/12\pi = \sigma^2\Delta\gamma = -\sigma^2\mathcal{S}$, which may be more familiar to those working in colloid science (Israelachvili 1992) and thin-film fluid dynamics (deGennes 1985). In direct analogy with the wetting of an inert wall by a liquid phase, the driving force for wetting of the solid by its own melt phase is the reduction in interfacial free energy. For interfacial melting, the interface in question melts because the "dry" interfacial energy is greater than the combined energies of the two new interfaces: $\Delta\gamma < 0$ and hence $\mathcal{A} < 0$ and $\mathcal{S} > 0$. Yet, additionally, such coefficients embody long-ranged intermolecular forces that underlie the cohesion of the surface film and its adhesion to the solid. If those forces are frequency-dependent van-der-Waals or dispersion interactions, this is embodied in the dielectric properties of all three materials in the layered system and can have either sign: the film grows ($\mathcal{A} < 0$) or is not present ($\mathcal{A} > 0$) (Elbaum & Schick 1991, Tabor 1991, Wilen et al. 1995). If, for example, $\mathcal{A} > 0$ then this can lead to rupturing of a liquid film on a solid substrate when the interfacial interaction, or disjoining pressure, is attractive (e.g., de Gennes 1985, Thiele 2003).

We are interested in cases in which $\mathcal{A} < 0$ so that there is a force of repulsion (disjoining pressure) between the media bounding the liquid film, or the liquid film is attracted to the solid with a greater force than is the other phase. The external pressure applied to the third phase p_w, equal to that applied to the solid p_s, balances the thermomolecular pressure $p_T = -\mathcal{A}/6\pi h^3$, written here for nonretarded van-der-Waals forces, and the hydrodynamic pressure p_l, giving

$$p_w = p_s = p_T + p_l. \tag{3.12}$$

Combining Equation 3.12 with the Gibbs-Duhem relationship (Equation 3.3), setting $\rho_s = \rho_l$, and using the form of the disjoining pressure above, shows that the equilibrium thickness of the liquid film is

$$h = \lambda \left(\frac{T_m - T}{T_m} \right)^{-1/3}, \tag{3.13}$$

where $\lambda^3 = -\mathcal{A}/6\pi\rho_s\mathcal{L}$. Equation 3.13 shows that for $\mathcal{A} < 0$ a premelted liquid film exists at temperatures below the bulk melting point and its thickness grows with temperature. This description of interfacial premelting is that which has received detailed experimental confirmation for many different materials (Dash et al. 1995).

Equation 3.13 shows that the thickness of a premelted liquid film increases as the temperature increases and, hence, the thermomolecular pressure decreases. Therefore, when the external pressure is held constant, the pressure in the liquid increases with temperature and there is a tendency for premelted liquid to flow from warmer to cooler regions. We explore the varied fluid mechanical phenomena associated with this tendency in the next section.

The two ideas described above—curvature melting and interfacial premelting—can be combined in a single thermodynamic treatment to derive the generalized Clapeyron relationship
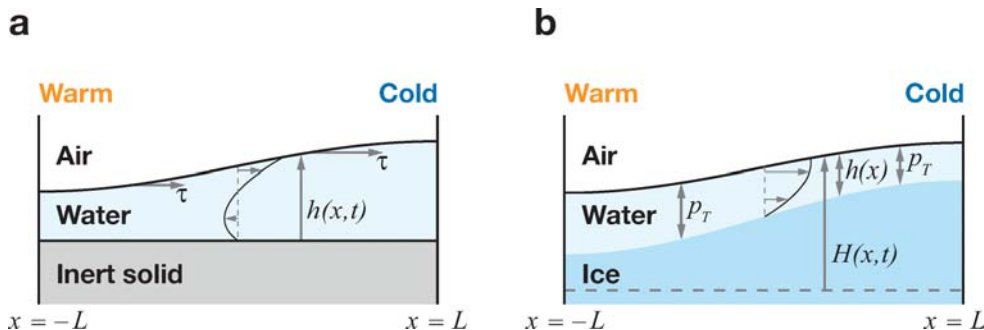
$$\rho_s \mathcal{L} \frac{T_m - T}{T_m} = (p_l - p_m)\left(1 - \frac{\rho_s}{\rho_l}\right) + p_T(h) + \gamma_{sl}\mathcal{K}, \tag{3.14}$$

(e.g., Baker & Dash 1989, Rempel et al. 2004, Rempel & Worster 2001). We shall ignore the first term on the right-hand side (corresponding to pressure melting and justified in the discussion following Equation 3.4) throughout, but explore the combined effects of interfacial premelting and curvature beginning in Section 5.

4. FLOWS DRIVEN BY DISJOINING FORCES

The flows with which we are concerned seem similar to, but are fundamentally distinct from, the more familiar Marangoni, or thermocapillary, flows driven by gradients of surface tension at a free surface. To make this distinction, consider the two situations depicted in **Figure 3**.

Figure 3a shows a thin layer of water sitting on a rigid, nonreacting boundary. The imposed horizontal temperature gradient induces a gradient in the surface tension of the water-air interface and a net surface traction $\tau = -\gamma'_{lv}\mathcal{G}$ toward the cold end of the system, where $\gamma_{lv} = \gamma_{lv}(T)$ is the surface tension between the liquid and vapor phases,

a

Warm   Cold

Air

τ

Water $h(x,t)$

Inert solid

$x = -L$ $x = L$

b

Warm   Cold

Air $h(x)$ p_T

Water p_T

Ice $H(x,t)$

$x = -L$ $x = L$

Figure 3

Schematics of thin-film flows. In (*a*) the flow is driven by Marangoni stresses, whereas in (*b*) the flow is driven by gradients in the thermomolecular pressure, or equivalently, the disjoining pressure.

γ'_{lv} is its derivative with respect to temperature, and $-\mathcal{G}$ is the imposed temperature gradient. The thickness $h(x, t)$ of the water film varies in time until the curvature-induced pressure drives a balancing counter flow. Note that even once the interface is stationary, the water continues its circulation. This situation can be modeled as follows.

Lubrication theory (Batchelor 2000) gives the horizontal velocity

$$u = \frac{-\gamma'_{lv}\mathcal{G}}{\mu}z - \frac{1}{2\mu}\frac{\partial p}{\partial x}z(2h - z) \qquad (4.1)$$

as a combination of a Couette flow driven by the surface traction and a Poiseuille flow driven by the curvature (or Laplace) pressure

$$p = -\gamma_{lv}h_{xx}, \qquad (4.2)$$

where μ is the dynamic viscosity of the water. The net horizontal flux of water is

$$q \equiv \int_0^h u\,dz = \frac{-\gamma'_{lv}\mathcal{G}}{\mu}h^2 + \frac{\gamma_{lv}h^3}{3\mu}h_{xxx}. \qquad (4.3)$$

Local mass conservation, expressed by $h_t + q_x = 0$, gives

$$h_t = \left[-\frac{-\gamma'_{lv}\mathcal{G}}{\mu}h^2 - \frac{\gamma_{lv}h^3}{3\mu}h_{xxx} \right]_x . \qquad (4.4)$$

This equation can be used to determine the evolution of $h(x, t)$ starting from an initial state, and shows that there is an ultimate steady state given approximately by

$$h = h_0 - \frac{-\gamma'_{lv}\mathcal{G}L^3}{4\gamma h_0}\left[\left(\frac{x}{L}\right)^3 - 3\frac{x}{L} \right] \qquad (4.5)$$

if $-\gamma'_{lv}(T)\mathcal{G}L^3/4\gamma h_0 \ll h_0$, i.e., if the interface deflection is small, where $2L$ is the length of the domain and h_0 is the thickness of the film at $x = 0$.

The situation depicted in **Figure 3b** similarly has a thin layer of water between air and a solid. This time, however, the solid is ice and, at temperatures below 0°C, the

water owes its existence to the van-der-Waals interactions between the three phases. The thickness $h(x)$ of the water film is determined thermodynamically by Equation 3.14 and is independent of time. The water still flows, giving a mass flux toward the cold end of the system as before, but changes phase as it does so to maintain thermodynamic equilibrium. For the purpose of this illustration, we assume that $\gamma'_{lv} = 0$ so that there is no surface traction. The flow is then given solely by the second term on the right-hand side of Equation 4.1, but now with

$$p = -\gamma_{lv} H_{xx} - \frac{\mathcal{A}}{6\pi h^3} = -\gamma_{lv} H_{xx} - \rho_s \mathcal{L} \frac{T_m - T}{T_m}, \tag{4.6}$$

where $H(x, t)$ is the position of the air-water interface and we neglect (for clarity here) the effect of the curvature of the ice-water interface on the film thickness. Mass conservation in this situation gives

$$H_t = \frac{\partial}{\partial x} \left(\frac{h^3}{3\mu} \frac{\partial p}{\partial x} \right) = \frac{\partial}{\partial x} \left[\frac{h^3}{3\mu} \left(-\gamma_{lv} H_{xxx} - \frac{\rho_s \mathcal{L} \mathcal{G}}{T_m} \right) \right]. \tag{4.7}$$

Thus, there is horizontal mass transport until the curvature pressure balances the thermomolecular pressure. The steady state is given approximately by

$$H = H_0 - \frac{\rho_s \mathcal{L} \mathcal{G} L^3}{\gamma_{lv} T_m} \left[\left(\frac{x}{L} \right)^3 - 3 \frac{x}{L} \right], \tag{4.8}$$

which is comparable to Equation 4.5. Note, however, that in this steady state there is no further fluid motion.

By comparing Equation 4.5 with Equation 4.8, we see that the Marangoni effect dominates the effect of gradients in disjoining forces if

$$h_0 \ll \frac{-\gamma'_{lv} T_m}{\rho_s \mathcal{L}} = h_c. \tag{4.9}$$

Typical values give $h_c \approx 10^{-7}$m, which is the scale below which van-der-Waals forces tend to be significant in other contexts. However, the thermomolecular flows continue to operate when the air in the previous examples is replaced by an inert solid and its interface with the water film is no longer hydrodynamically free, so that Marangoni effects are entirely absent. It is to these novel situations that the remainder of this article is devoted.

For example, Wilen & Dash (1995) designed an experiment to investigate the flow of premelted liquid in which a disk of ice was formed in the horizontal gap between a lower glass slide and an upper flexible membrane (**Figure 4a**). The steady temperature increased linearly with radius, and the outer edge of the disk corresponded with the 0°C isotherm. The thermomolecular pressure gradient described above drew water radially inward, between the ice disk and the upper membrane, which froze onto the upper surface of the disk and deflected the membrane upward (**Figure 4b**). The deflection was monitored continuously using an interference microscope.

Because all the action occurs very close to the edge of the disk, this experiment can be analyzed with a two-dimensional model similar to that described above. Various intermolecular interactions play a role in controlling the relationship between film thickness and temperature, and hence modify Equation 3.13. For illustration here,
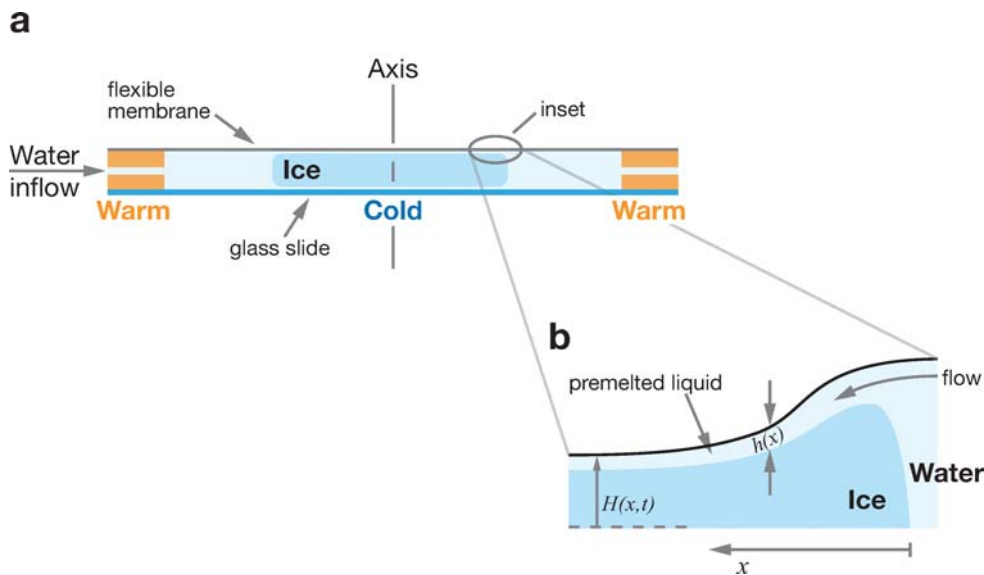
Figure 4

(*a*) Schematic of the experimental set up of Wilen & Dash (1995). (*b*) Inset showing fluid flow and deflection of the membrane. See text for more detail.

we consider only nonretarded van der Waals interactions. Then, if x is measured radially inward from the 0°C isotherm, so that $T = T_m - \mathcal{G}x$, Equation 4.7 can be written as

$$H_t + D[x^{-1}(H_{xxx} + \alpha)]_x = 0, \tag{4.10}$$

where

$$D = \frac{1}{12}\frac{\lambda^3 T_m}{\mathcal{G}}\frac{\gamma}{\mu}, \quad \alpha = \frac{\rho_s \mathcal{L}\mathcal{G}}{T_m\gamma} \tag{4.11a,b}$$

and γ is the constant tension in the elastic membrane.[3] Equation 4.10 admits a similarity solution

$$h = \alpha(Dt)^{3/5}f(\eta), \quad \text{with} \quad \eta = x/(Dt)^{1/5} \tag{4.12a,b}$$

and

$$f'''' - (f''' + 1)/\eta - \frac{1}{5}\eta^2 f' + \frac{3}{5}\eta f = 0, \tag{4.13}$$

where the primes denote $d/d\eta$. These equations are subject to the boundary conditions

$$f' = f'' = 0 \quad (\eta = 0), \quad f, f' \to 0 \quad (\eta \to \infty), \tag{4.14}$$

and the solution is displayed in **Figure 5** in comparison with the experimental data.

---

[3]Note that the factor $\frac{1}{3}$ in Equation 4.8 is replaced by $\frac{1}{12}$, which is a consequence of applying the no-slip condition at the membrane.
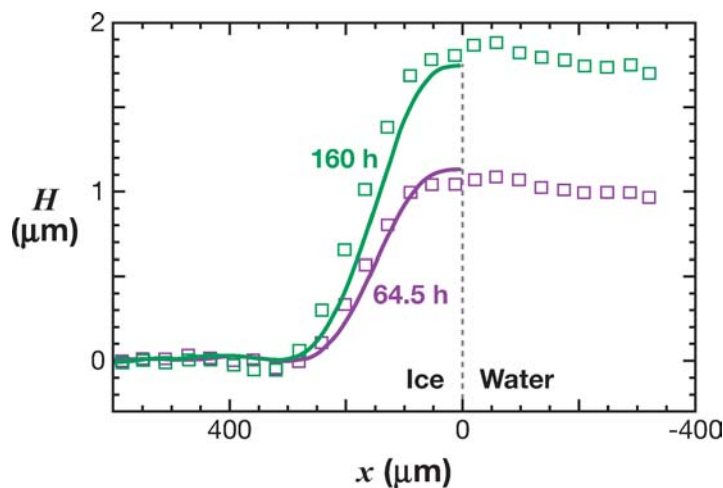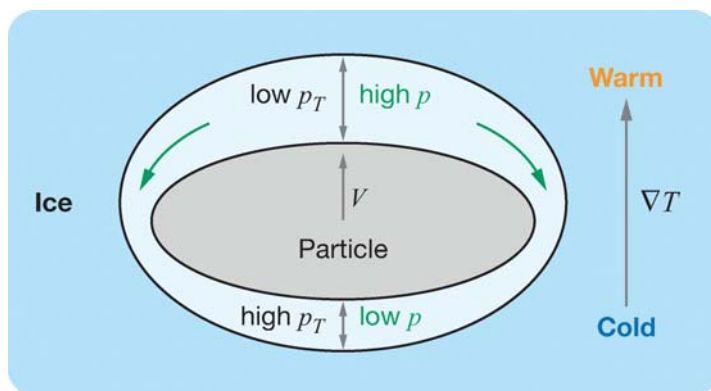
Figure 5

Similarity solution in comparison with experimental data.

For a given interaction, all of the physical parameters in this theory are known independently of the experiments of Wilen & Dash (1995), with the exception of λ, which characterizes the nature and strength of the forces underlying interfacial premelting. Additionally, it has often been speculated that, although premelted liquid behaves as a Newtonian fluid sufficiently close to T_m (Mantovani et al. 1980, Tsionsky et al. 2002), its viscosity can be much larger than that of bulk supercooled water and at lower temperatures may become non-Newtonian (Tsionsky et al. 2003). Yet experiments on water confined between interfaces of mica reveal a constant shear viscosity down to the scale of just a few molecules (Raviv & Klein 2002) despite the potential ordering effect of the underlying solid (see Zhu & Granick 2003 and references therein). Because λ and μ only appear in ratio, in the parameter D, it is not possible to use these experiments to determine values for λ and μ separately. However, because $T \approx T_m$, it is assumed that the viscosity of the premelted liquid is the same as that of bulk liquid and a prediction for λ can be made (Wettlaufer et al. 1996) that is consistent with independent calculations of the interactions (Wilen et al. 1995). A similar inference was drawn by Gilpin (1980a) from wire-regelation experiments, which are discussed below.

5. THERMODYNAMIC BUOYANCY AND THE PHENOMENON OF REGELATION

We have seen that thermomolecular flows are driven by gradients in normal stresses, unlike Marangoni flows, which are driven by tangential stresses. We have looked at cases in which one boundary of the premelted film is deformable and for which, therefore, the flow can be determined locally by continuity, Equation 4.4. However, there are many circumstances in which both boundaries of the film are dynamically

Figure 6

Schematic of thermal regelation.

rigid, in which case the pressure field can only be determined from a global force balance.

The canonical example is that of a rigid particle embedded in a solid material that is close to its bulk melting temperature (**Figure 6**). Then, as long as the solid premelts against the particle, the imposition of a temperature gradient will cause the particle to move by a process of melting and refreezing referred to as thermal regelation. Tyndall (1858) and Faraday (1860) used the term regelation to describe the sintering of ice crystals by the freezing of (premelted) liquid layers on their surfaces. Thermal regelation was first modeled by Gilpin (1979) alongside the closely related phenomenon of pressure-induced regelation, by which a weighted wire can be pulled through a block of ice. Although the latter can be effected by pressure melting (the decrease in bulk freezing temperature of ice under pressure), Telford & Turner (1963) showed that regelation still occurs at temperatures and pressures at which pressure melting is not operative. Interfacial premelting explains both pressure-induced regelation and thermal regelation, as described by Worster & Wettlaufer (1999), and here we illustrate the essential aspects of the process.

The net thermomolecular force on the particle, arising from the intermolecular interactions, is

$$\mathbf{F}_T \equiv -\int_\Gamma p_T \, d\Gamma = \int_\Gamma \left(\gamma_{sl} \mathcal{K} - \rho_s L \frac{T_m - T}{T_m} \right) d\Gamma, \qquad (5.1)$$

where the surface area element $d\Gamma$ points in the direction of the outward normal to the particle (Rempel et al. 2001a, 2004). Because the surface Γ of the particle is closed, the integral of the curvature term is zero, and application of the divergence theorem gives

$$\mathbf{F}_T = \frac{\rho_s \mathcal{L}}{T_m} \int_{\mathcal{D}} \nabla T \, dV, \qquad (5.2)$$

where $\mathcal{D}$ is the interior of Γ. This force can be written as

$$\mathbf{F}_T = m_s \frac{\mathcal{L}}{T_m} \langle \nabla T \rangle = m_s \mathbf{G}, \qquad (5.3)$$

in which $\langle \nabla T \rangle$ is the mean of the temperature gradient over the interior of the particle, m_s is the mass of solid displaced by the particle, and $\mathbf{G} \equiv (\mathcal{L}/T_m)\langle \nabla T \rangle$. Certainly, when the particle and surrounding solid have different thermal conductivities, the mean internal temperature gradient may be a function of the conductivity ratio and the geometry of the particle. However, such complications are not fundamental to the mechanism of regelation and its applications to the freezing of porous media. We therefore take the conductivities to be equal so that $\mathbf{G} = (\mathcal{L}/T_m)\nabla T$, where ∇T is the applied temperature gradient.

The importance of the simple result (Equation 5.3) is that the net thermomolecular force is independent of the curvature and independent of the type and strength of the intermolecular interactions giving rise to p_T. Furthermore, the net force is simply proportional to the mass of displaced solid (ice), which is central both to the conceptual framework of regelation as a kind of thermodynamic buoyancy and to our understanding of frost heave.

The rate at which the particle can move in response to the thermomolecular force is controlled by the necessary viscous flow in the premelted film. That flow depends on the thickness and geometry of the film, which depend on surface energy and curvature as well as the strength of the intermolecular interactions. The hydrodynamic forces on the particle are dominated by the lubrication pressure, which must be integrated over the surface of the particle.

For simple geometries the flow can readily be calculated. For example, if the particle is a sphere of radius a and only nonretarded van-der-Waals interactions are considered, the net lubrication force is

$$\mathbf{F}_\mu = -\frac{4\pi a^3}{3}\frac{6\mu a\mathbf{V}}{\lambda^3}\left(\frac{T_m - T_0}{T_m}\right), \tag{5.4}$$

when the particle is moving with velocity $\mathbf{V}$ (Rempel et al. 2004, Worster & Wettlaufer 1999), where T_0 is the temperature at the center of the particle.

If the sphere is heavier than the premelted liquid, then there is an "overburden" force

$$\mathbf{F}_O = -\frac{4\pi a^3}{3}\Delta\rho\mathbf{g}, \tag{5.5}$$

where $\Delta\rho$ is the density difference between particle and water, and g is the gravitational acceleration. In mechanical equilibrium, the total force $F_T + F_\mu + F_O$ is zero, so the migration velocity can be determined to be

$$\mathbf{V} = \frac{\lambda^3}{6\mu a}\frac{T_m}{T_m - T_0}[\rho_s\mathbf{G} - \Delta\rho\mathbf{g}]. \tag{5.6}$$

This simple expression illustrates the processes of thermal regelation ($\mathbf{g} = 0$) and pressure-induced regelation ($\mathbf{G} = 0$)—although without pressure melting—and shows the dominant physical parameters controlling these phenomena. To make quantitative comparisons with experiments, however, a more detailed analysis is required that accounts for a conductivity ratio that differs from unity, a variety of intermolecular forces, compositional and latent heat effects, and pressure melting (e.g., Nye 1967). Searches for the presence of interfacial premelting in materials

other than ice may be most fruitfully studied by quantitative investigation of particle motion, and efforts along these lines are still underway.

The same underlying physical phenomena just described explain how, during the solidification of a fluid in which insoluble particles are dispersed, the solid phase can be devoid of those particles. Experiments show that if the mixture is frozen at a rate greater than a critical value V_c, then the particles are trapped in the solid phase, whereas at rates slower than V_c, they are pushed ahead of the phase boundary and remain in the fluid (e.g., Azouni et al. 1990, Lipp et al. 1990, Lipp & Körber 1993).

The classical treatment of the rejection process assumes the phase boundary to be planar and analyzes the squeeze film between the pushed, spherical particle and the solid material under the influence of a van-der-Waals repulsion. It is then postulated that the particle is captured only when it reaches a molecular distance from the phase boundary.

However, once the particle is sufficiently close to come under the influence of long-range intermolecular interactions, the solid-liquid interface adopts the shape dictated by Equation 3.15 and conforms to the particle (**Figure 7**). This increases the lubrication force significantly and, once it can no longer be balanced by the van-der-Waals repulsion, the particle becomes engulfed.

This fundamental mechanism was understood by Chernov et al. (1977), who made approximate predictions for V_c by assuming that the phase boundary is paraboloidal or comprises the union of a truncated paraboloid and a plane, as illustrated in **Figure 7**. Gilpin (1980b) attempted to improve upon this analysis using matched asymptotics to capture the shape of the shoulder regions where the interface bends back to the outer plane. However, Rempel & Worster (1999, 2001) showed that the critical velocity can be determined simply by integral constraints without determining the interface shape explicitly. The steady pushing velocity is thereby

$$V = \frac{A}{36\pi\mu a} \frac{d_0^3}{d_0^4 + 3l^4}, \tag{5.7}$$

where $l^4 = \lambda^3 T_m/\mathcal{G}$, d_0 is the minimum thickness of the liquid film and $\mathcal{G}$ is the magnitude of the uniform temperature gradient. This expression is plotted in **Figure 7**, where it is compared with the results of Chernov el al. (1977), and with results obtained by assuming the interface to be spherical or planar. The critical velocity

$$V_c = \frac{\sqrt{3}}{144\pi} \frac{A}{\mu al} = \frac{\sqrt{3}}{24} \frac{\rho_s \mathcal{L}\lambda^{9/4}}{\mu T_m^{1/4}} \frac{\mathcal{G}^{1/4}}{a} \tag{5.8}$$

is obtained by maximizing V with respect to d_0.

First, we note that at the critical solidification rate $d_0 = \sqrt{3}l$, whereas the deflection of the interface is only $l/3\sqrt{3}$, so the particle sits above the undisturbed position of the interface, as shown in **Figure 7**. Second, there is significant experimental support for the relationship $V_c \propto a^{-1}$ and some support for the relationship $V_c \propto \mathcal{G}^{1/4}$, although there is also evidence in favor of other exponents in the latter expression (Lipp & Körber 1993, Pötschke & Rogge 1989). Third, because the critical solidification rate provides a different relationship between viscosity and the Hamaker constant, then in principle it can be used in combination with the earlier result (Equation 5.6) to
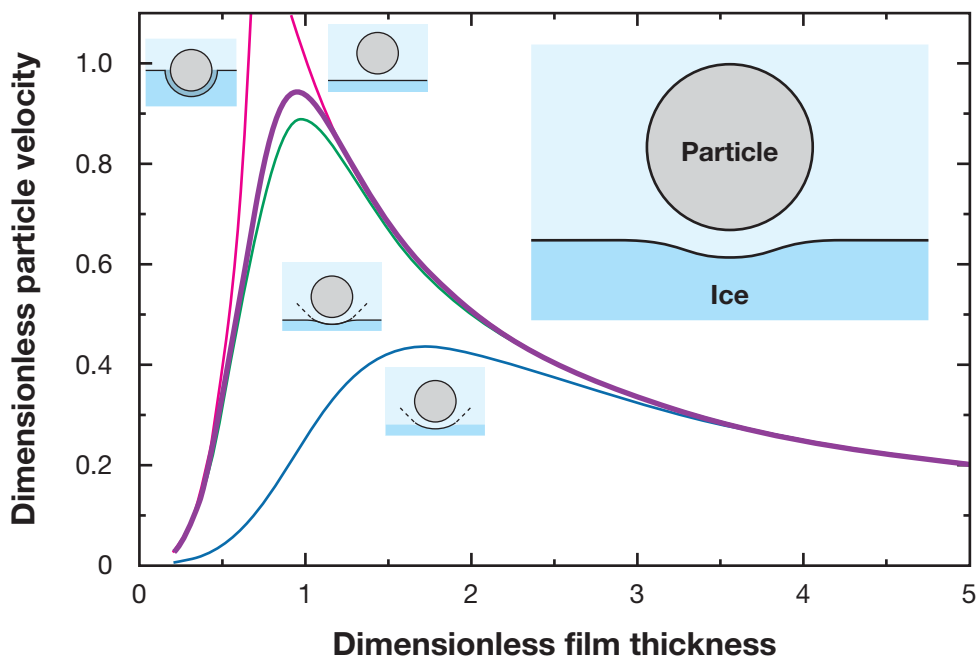
Figure 7

Dimensionless particle velocity as a function of the dimensionless film thickness. The thick
purple line shows the leading-order behavior that is predicted by the complete theory,
including interfacial curvature, which, for large film thicknesses, is nearly identical to the
results obtained when approximating the phase boundary as being planar (*rightmost magenta
curve*). The leftmost magenta curve gives the approximate velocity when the temperature on
the particle surface is substituted for that along the phase boundary. The green curve displays
the predictions of Chernov et al. (1977) for the case where the interface has the form of a
paraboloid intersecting with a plane, and the lowest (*blue*) curve is their prediction for the
particle velocity when the phase boundary is modeled as a paraboloid.

determine values for these quantities separately. Moreover, although the trapping
process is not instantaneous, the particle is typically only pushed some fraction of its
radius before engulfment (Rempel & Worster 1999).

It is often the case that the interfacial deflection is affected by dissolved impurities
or to differing thermal conductivities of ice and particle, which can, for example,
enhance rejection if the particle is less conductive than the ice (Chernov et al. 1977).
However, although quantitative experimental measurements are still evolving, recent
studies (Azouni et al. 1997) suggest that bulk thermal effects are not the primary
mechanism controlling engulfment, but rather the process is dominated by the nature
of the surface of the particle, as described above.

6. FROST HEAVE

The ideas of the previous section are fundamental to the underlying mechanisms
of frost heave, by which saturated soils expand as they freeze, causing damage to

engineering structures (e.g., Palmer & Williams 2003) and giving rise to some beautiful geomorphological features (Hallet 1990). We have seen that particles immersed in ice migrate up temperature gradients and can be rejected by ice as it solidifies. When saturated soil freezes, the ice that forms pushes down on the soil particles, but the effect is that the ice is pushed upward. Near the surface, this can give rise to needle ice (**Figure 8**). Below the surface, the ice tends to form horizontal lenses that are devoid of soil particles (Taber 1929, 1930). It is the dynamics of premelting at the surface of and around ice lenses, rather than the expansion of water as it freezes, that is responsible for frost heave. Heaving occurs even when the saturating liquid contracts on freezing. This was first demonstrated by Taber (1929), who performed experiments on a soil saturated with benzene, and more recently by experiments in which helium (Mizusaki & Hiroi 1995) and argon (Zhu et al. 2000) were solidified in porous glass and silica powder, respectively.

The dynamics of a single lens was analyzed on the scale of the soil grains by Worster & Wettlaufer (1999), who considered a periodic array of spherical particles being rejected by an ice front, analogous to the situation depicted in **Figure 7**. However, more useful and generalizable macroscopic theories can be developed in terms of the thermodynamic buoyancy described above.

Consider, for example, the situation depicted in **Figure 9**. A saturated soil is cooled from above and has frozen (perhaps only partially) down to an ice lens whose lower boundary is at $z = 0$, where the temperature is equal to T_0. As more water is frozen onto the bottom of the ice lens, thermomolecular forces push the lens upward and create the hydraulic pressure needed to draw water through the porous soil below up to the freezing front. We imagine that the temperature and pressure have fixed values T_H and p_H at $z = H$, and $T = T_S$, $p = 0$ at the surface $z = -b(t)$.

Frost heave is a very slow process, so for simplicity we assume that the temperature field is quasi-steady and therefore piecewise linear. Conservation of heat at the ice
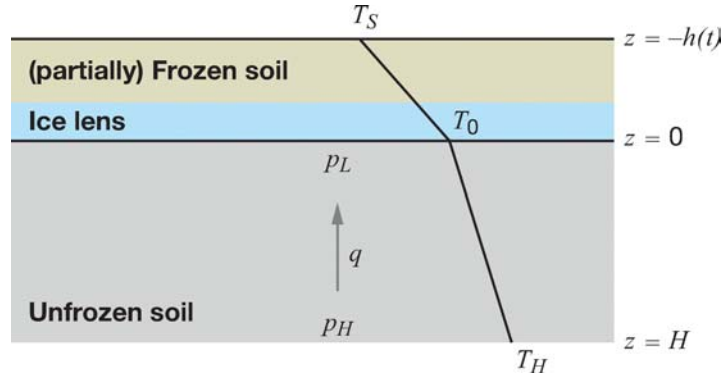
Figure 9

Frost heave caused by an ice lens with no frozen fringe.

lens requires that the Stefan condition

$$\rho_s \mathcal{L} \dot{h} = k \frac{T_0 - T_S}{h} - k \frac{T_H - T_0}{H} \tag{6.1}$$

be satisifed, where k is the thermal conductivity, here assumed independent of material and phase.

Conservation of mass requires that the upward flux of water q through the porous, unfrozen soil is equal to the rate of heave $\dot{h}$, again neglecting for simplicity the density difference between water and ice, and Darcy's law gives

$$\dot{h} = -\Pi(p_H - p_L), \tag{6.2}$$

which determines the liquid pressure p_L just below the ice lens, where Π is the permeability of the soil.

Finally, the frost-heaving pressure on the ice lens is determined by thermodynamic buoyancy to be

$$p_T = \rho_s \mathcal{L}(T_m - T_0)/T_m. \tag{6.3}$$

The net force on the ice lens $p_T + p_L + p_O$ must be zero, where $p_O = \rho g h$ is the overburden pressure, so

$$\dot{h} = \Pi \left[p_H + \rho_s \mathcal{L}(T_m - T_0)/T_m - \rho g h \right]. \tag{6.4}$$

For slow heaving, we can neglect the left-hand side of Equation 6.1, solve it algebraically for T_0, and then solve the differential Equation 6.4, which can be written nondimensionally as

$$h_\tau = h_H - h + \Gamma(1 + \theta h)/(1 + h), \tag{6.5}$$

where h has been scaled with H, $\tau = \rho g \Pi t$, $h_H = p_H/\rho g H$, $\theta = (T_H - T_m)/\Delta T$, $\Gamma = \rho_s \mathcal{L} \Delta T/\rho g H T_m$, and $\Delta T = (T_m - T_S)$. Although Equation 6.5 can be solved straightforwardly, the resulting general analytic expression is not particularly informative. Its character is illustrated by the special case $\theta = 1$, when

$$h = (h_H + \Gamma)(1 - e^{-\tau}). \tag{6.6}$$

This shows that the surface of the ground heaves until, in dimensional terms, the overburden pressure at the bottom of the lens $\rho g b$ is balanced by the maximum frost-heaving pressure $\rho g \Gamma = \rho_s \mathcal{L} \Delta T / T_m$ plus the imposed hydraulic head p_H.

This model can be contrasted with the model of primary frost heave with frost penetration developed by O'Neill & Miller (1985) and described by Fowler (1997), in which the interfacial temperature T_0 is determined as the temperature T_f at which the mean radius of curvature of the microscopic ice meniscus, as given by Gibbs-Thomson, is equal to the mean size of the throats between soil grains. Here we see that the interfacial temperature is determined dynamically by considering the net thermodynamic buoyancy on the ice lens.

If, by the analysis described above, the interfacial temperature T_0 is predicted to be less than T_f, then a partially frozen "fringe" can form separating the ice lens from unfrozen soil. The volume fraction ϕ occupied by ice in the fringe is determined thermodynamically, $\phi = \phi(T)$, and the dynamics of heaving are determined by the same fundamental balance between thermodynamic buoyancy, lubrication pressure, and overburden pressure as before. The first two of these can be expressed as volume integrals dependent on ϕ (Rempel et al. 2004), showing that the microscopic morphology enters only in the determination of the permeability of the fringe. This is a strongly nonlinear function of ϕ, and hence of position. Consequently, a local minimum of the "effective pressure" between soil grains occurs within the fringe, and if the minimum value is sufficiently small then the soil grains can separate to form a new lens. This is the fundamental mechanism proposed by O'Neill & Miller (1985) in their model of "secondary frost heave." It was analyzed by Fowler & Krantz (1994) and more simply by Rempel et al. (2004) to make predictions of the periodic lensing observed in experiments (Taber 1929). Similar thinking along the lines of Rempel et al. (2004) has been applied to frost-heave experiments in quartz capillaries by Churaev (2004). An important outstanding aspect of the dynamics of frozen media concerns the space-time evolution of ϕ, and hence the underlying forces that control the rheology of the matrix.

7. CONCLUSIONS

When Tyndall (1858) and Faraday (1860) proposed the idea of surface melting as an explanation of the sintering of ice crystals in snowballs, it was simply an hypothesis, which lost favor in the face of Kelvin's ideas of pressure melting. It is now known that both mechanisms have a firm basis in thermodynamics, expressed in a generalized Clapeyron relationship (Equation 3.14), and have been observed experimentally. There are interesting fluid mechanical phenomena associated with surface and interfacial melting, in which free surfaces are determined thermodynamically but net forces are strongly influenced by the ability of the molten films to flow. Much of the action occurs on submicron scales yet has large-scale geophysical consequences and industrial applications. Future research involving the fundamental mechanisms described in this article can be imagined in areas as diverse as the cryopreservation of biological tissue and atmospheric chemistry in polar stratospheric clouds. In all these fields the fluid dynamicist has an important role to play.

ACKNOWLEDGMENTS

LITERATURE CITED

Azouni MA, Casses P, Sergiani B. 1997. Capture or repulsion of treated nylon particles by an ice-water interface. *Colloids Surf. A* 122:199–205

Azouni MA, Kalita W, Yemmou M. 1990. On the particle behaviour in front of advancing liquid–ice interface. *J. Cryst. Growth* 99:201–5

Baker MB, Dash JG. 1989. Thunderstorm electrification and collisional charging of ice. *J. Cryst. Growth* 97:770–76

Barer SS, Deryagin BV, Kiseleva OA, Sobolev VD, Churaev NV. 1977. Study of thin interlayers between ice and surface of Quartz capillaries. *Colloid J. USSR* 39:917–21

Batchelor GK. 2000. *An Introduction to Fluid Dynamics*. Cambridge, UK: Cambridge Univ. Press

Beaglehole D, Nason D. 1980. Transition layer on the surface of ice. *Surf. Sci.* 96:357–63

Beaglehole D, Wilson P. 1994. Extrinsic premelting at the ice-glass interface. *J. Phys. Chem.* 98:8096–100

Bednorz A, Napiorkowski M. 2000. The problem of uniqueness in the reduced description of adsorption on the wedge-shaped substrate. *J. Phys. A* 33:L353–56

Benatov L, Wettlaufer JS. 2004. Abrupt grain boundary melting in ice. *Phys. Rev. E* 70:061606

Bluhm H, Ogletree DF, Fadley CS, Hussain Z, Salmeron M. 2002. The premelting of ice studied with photoelectron spectroscopy. *J. Phys. Cond. Matter* 14:L227–33

Boxe CS, Colussi AJ, Hoffmann MR, Tan D, Mastromarino J, et al. 2003. Multiscale ice fluidity in NOx photodesorption from frozen nitrate solutions. *J. Phys. Chem. A* 107:11409–13

Broughton JQ, Gilmer GH. 1986. Thermodynamic criteria for grain-boundary melting–a molecular dynamics study. *Phys. Rev. Lett.* 56:2692–95

Cahn JW. 1991. Stability, microstructural evolution, grain-growth and coarsening in a 2-dimensional 2-phase microstructure. *Acta Metall.* 39:2189–99

Campen RK, Sowers T, Alley RB. 2003. Evidence of microbial consortia metabolizing within a low-latitude mountain glacier. *Geology* 31:231–34

Chernov AA, Temkin DE, Mel'nikova AM. 1977. The influence of the thermal conductivity of a macroparticle on its capture by a crystal growing from a melt. *Sov. Phys. Crystallogr.* 22:656–58

Cho H, Shepson PB, Barrie LA, Cowin JP, Zaveri R. 2002. NMR investigation of the quasi-brine layer in ice/brine mixtures. *J. Phys. Chem. B* 106:11226–32

Churaev NV. 2004. Mass transfer in frozen porous bodies. *Colloid J.* 66:751–55

Dash JG. 2002. Melting from one to two to three dimensions. *Contemp. Phys.* 43:427–36

Dash JG, Fu H-Y, Wettlaufer JS. 1995. The premelting of ice and its environmental consequences. *Rep. Prog. Phys.* 58:115–67

Dash JG, Rempel AW, Wettlaufer JS. 2006. Physics, chemistry and geophysics of aqueous films on premelted ice. *Chem. Rev.* In press

Davis SH. 2001. *Theory of Solidification.* Cambridge, UK: Cambridge Univ. Press

deGennes PJG. 1985. Wetting: statics and dynamics. *Rev. Mod. Phys.* 57:827–63

deGennes PJG, Brochard-Wyart F, Quéré D. 2004. *Capillarity and Wetting Phenomena: Drops, Bubbles, Pearls, Waves.* New York: Springer-Verlag

Dietrich S. 1988. In *Phase Transition and Critical Phenomena*, ed. C Domb, JL Lebowitz, Vol. 12. pp. 1–218. London: Academic

Doppenschmidt A, Butt HJ. 2000. Measuring the thickness of the liquid-like layer on ice surfaces with atomic force microscopy. *Langmuir* 16:6709–14

Dosch H, Lied A, Bilgram JH. 1995. Glancing angle x-ray scattering studies of the premelting of ice surfaces. *Surf. Sci.* 327:145–64

Eastman T, Zhu D-M. 1995. Influence of an AFM tip on interfacial melting on ice. *J. Colloid Interface Sci.* 172:297–301

Elbaum M, Lipson SG, Dash JG. 1993. Optical study of surface melting on ice. *J. Cryst. Growth* 129:491–505

Elbaum M, Schick M. 1991. Application of the theory of dispersion forces to the surface melting of ice. *Phys. Rev. Lett.* 66:1713–16

Engemann S, Reichert H, Dosch H, Bilgram J, Honkimäki V, Snigirev A. 2004. Interfacial melting of ice in contact with SiO_2. *Phys. Rev. Lett.* 92:205701

Ewing GE. 2004. Thin film water. *J. Phys. Chem. B* 108:15953–61

Faraday M. 1860. Note on regelation. *Proc. R. Soc.* 10:440–50

Fowler AC. 1997. *Mathematical Models in the Applied Sciences.* Cambridge, UK: Cambridge Univ. Press

Fowler AC, Krantz WB. 1994. On the O'Neill/Miller model for secondary frost heave. *SIAM J. Appl. Math.* 54:1650–75

Furukawa Y, Yamamoto M, Kuroda T. 1987. Ellipsometric study of the transition layer on the surface of an ice crystal *J. Cryst. Growth* 82:665–77

Gilpin RR. 1979. A model of the "liquid-like" layer between ice and a substrate with applications to wire regelation and particle migration. *J. Colloid Interface Sci.* 68:235–51

Gilpin RR. 1980a. A model for the prediction of ice lensing and frost heave in soils. *Water Resourc. Res.* 16:918–30

Gilpin RR. 1980b. Theoretical studies of particle engulfment. *J. Colloid Interface Sci.* 74:44–63

Girardet C, Toubin C. 2001. Molecular atmospheric pollutant adsorption on ice: a theoretical survey. *Surf. Sci. Rep.* 44:163–238

Hallet B. 1990. Self-organization in freezing soils–from microscopic ice lenses to patterned-ground. *Can. J. Phys.* 68:842–52

Huthwelker T, Lamb D, Baker M, Swanson B, Peter T. 2001. Uptake of SO_2 by polycrystalline water ice. *J. Colloid Interface Sci.* 238:147–59

Ishizaki T, Maruyama M, Furukawa Y, Dash JG. 1996. Premelting of ice in porous silica glass. *J. Cryst. Growth* 163:455–60

Israelachvili JN. 1992. *Intermolecular and Surface Forces*. New York: Academic

Khvorostyanov VI, Curry JA. 2004. Thermodynamic theory of freezing and melting of water and aqueous solutions. *J. Phys. Chem. A* 108:11073–85

Kikuchi R, Cahn JW. 1980. Grain-boundary melting transition in a two-dimensional lattice-gas model. *Phys. Rev. B* 21:1893–97

Lipowsky R. 1982. Critical surface phenomena at first-order bulk transitions. *Phys. Rev. Lett.* 49:1575–78

Lipp G, Körber Ch. 1993. On the engulfment of spherical particles by a moving ice–liquid interface. *J. Cryst. Growth* 130:475–89

Lipp G, Körber Ch, Rau G. 1990. Critical growth rates of advancing ice–water interfaces for particle rejection. *J. Cryst. Growth* 99:206–10

Mader H. 1992a. Observations of the water-vein system in polycrystalline ice. *J. Glaciol.* 38:333–47

Mader H. 1992b. The thermal behavior of the water-vein system in polycrystalline ice. *J. Glaciol.* 38:359–74

Mantovani S, Valeri S, Loria A, del-Pennino U. 1980. Viscosity of the ice surface layer. *J. Chem. Phys.* 72:1077–83

Mizusaki T, Hiroi M. 1995. Frost heave in He. *Physica B* 210:403–10

Netz RR, Andelman D. 1997. Roughness-induced wetting. *Phys. Rev. E* 55:687–700

Nye JF. 1967. Theory of regelation. *Philos. Mag.* 16:1249–66

Nye JF. 1991. Thermal behavior of glacier and laboratory ice. *J. Glaciol.* 37:401–13

Nye JF. 1992. Water veins and lenses in polycrystalline ice. In *Physics and Chemistry of Ice*, ed. N Maeno, T Hondoh, pp. 200–5. Sapporo: Hokkaido Univ. Press

Nye JF, Frank FC. 1973. Hydrology of the intergranular veins in a temperate glacier. In *International Association of Scientific Hydrology Publication. Symp. Cambridge 1969: Hydrol. Glaciers* 95:157–61

O'Neill K, Miller RD. 1985. Exploration of a rigid ice model of frost heave. *Water Resour. Res.* 21:281–86

Oxtoby DW. 2002. Density functional methods in the statistical mechanics of materials. *Annu. Rev. Mater. Res.* 32:39–52

Oxtoby DW. 2003. Crystal nucleation in simple and complex fluids. *Philos. Trans. R. Soc. London Ser. A* 361:419–27

Palmer AC, Williams PJ. 2003. Frost heave and pipeline upheaval buckling. *Can. Geotech. J.* 40:1033–38

Pittenger B, Fain SC, Cochran MJ, Donev JMK, Robertson BE, et al. 2001. Premelting at ice-solid interfaces studied via velocity-dependent indentation with force microscope tips. *Phys. Rev. B* 63:134102

Pötschke J, Rogge V. 1989. On the behaviour of foreign particles at an advancing solid–liquid interface. *J. Cryst. Growth* 94:726–38

Rascon C, Parry AO. 2000. Geometry-dominated fluid adsorption on sculpted solid substrates. *Nature* 407:986–89

Raviv U, Klein J. 2002. Fluidity of bound hydration layers. *Science* 297:1540–43

Reif F. 1965. *Fundamentals of Statistical and Thermal Physics*. New York: McGraw-Hill

Rempel AW. 2000. *Dynamics of premelted films with geophysical applications*. PhD thesis. Univ. Cambridge, UK

Rempel AW, Waddington ED, Wettlaufer JS, Worster MG. 2001b. Possible displacement of the climate signal in ancient ice by premelting and anomalous diffusion. *Nature* 411:568–71

Rempel AW, Wettlaufer JS. 2003a. Segregation, transport, and interaction of climate proxies in polycrystalline ice. *Can. J. Phys.* 81:89–97

Rempel AW, Wettlaufer JS. 2003b. Isotopic diffusion in polycrystalline ice. *J. Glaciol.* 49:397–406

Rempel AW, Wettlaufer JS, Worster MG. 2001a. Interfacial premelting and the thermomolecular force: thermodynamic buoyancy. *Phys. Rev. Lett.* 97:088501

Rempel AW, Wettlaufer JS, Worster MG. 2004. Premelting dynamics in a continuum model of frost heave. *J. Fluid Mech.* 498:227–44

Rempel AW, Worster MG. 1999. The interaction between a particle and an advancing solidification front. *J. Cryst. Growth* 205:427–40

Rempel AW, Worster MG. 2001. Particle trapping at an advancing solidification front with interfacial-curvature effects. *J. Cryst. Growth* 223:420–32

Sadtchenko V, Ewing GE. 2002. Interfacial melting of thin ice films: an infrared study. *J. Chem. Phys.* 116:4686–97

Schick M. 1990. Introduction to wetting phenomena. In *Les Houches, Session XLVIII, 1988—Liquids at Interfaces*, ed. J Charvolin, JF Joanny, J Zinn-Justin, pp. 415–97. Amsterdam: Elsevier

Schick M, Shih WH. 1987. Z(N) model of grain boundary wetting. *Phys. Rev. B* 35:5030–35

Smith CS, Guttman L. 1953. Measurement of internal boundaries in 3-dimensional structures by random sectioning. *Trans. AIME* 197:81–87

Taber S. 1929. Frost heaving. *J. Geol.* 37:428–61

Taber S. 1930. The mechanics of frost heaving. *J. Geol.* 38:303–17

Tabor D. 1991. *Gases, Liquids and Solids and Other States of Matter*. Cambridge, UK: Cambridge Univ. Press.

Telford JW, Turner JS. 1963. The motion of a wire through ice. *Philos. Mag.* 8:527–31

Thiele U. 2003. Open questions and promising new fields in dewetting. *Eur. Phys. J. E* 12:409–16

Tsionsky V, Daikhin L, Zagidulin D, Urbakh M, Gileadi E. 2003. The quartz crystal microbalance as a tool for the study of a "liquid-like layer" at the ice/metal interface. *J. Phys. Chem. B* 107:12485–91

Tsionsky V, Zagidulin D, Gileadi E. 2002. Evidence for the existence of a "liquid-like layer" between a metal electrode and a frozen aqueous electrolyte. *J. Phys. Chem. B* 106:13089–93

Tyndall J. 1858. On some physical properties of ice. *Proc. R. Soc.* 9:76–80

Warren SG, Hudson SR. 2003. Bacterial activity in South Pole snow is questionable. *Appl. Environ. Microbiol.* 69:6340–41

Wei X, Miranda PB, Zhang C, Shen YR. 2002. Sum-frequency spectroscopic studies of ice interfaces. *Phys. Rev. B* 66:085401

Wettlaufer JS. 1999. Impurity effects in the premelting of ice. *Phys. Rev. Lett.* 82:2516–19

Wettlaufer JS, Worster MG. 1995. The dynamics of premelted films: frost heave in a capillary. *Phys. Rev. E* 51:4679–89

Wettlaufer JS, Worster MG, Wilen LA, Dash JG. 1996. A theory of premelting dynamics for all power law forces. *Phys. Rev. Lett.* 76:3602–5

Wilen LA, Dash JG. 1995. Frost heave dynamics at a single crystal interface. *Phys. Rev. Lett.* 74:5076–79

Wilen LA, Wettlaufer JS, Elbaum M, Schick M. 1995. Dispersion force effects in interfacial premelting of ice. *Phys. Rev. B* 52:12426–33

Worster MG, Wettlaufer JS. 1999. The fluid mechanics of premelted liquid films. In *Fluid Dynamics at Interfaces*, ed. W Shyy, R Narayanan, pp. 339–51. Cambridge, UK: Cambridge Univ. Press

Zhu D-M, Vilches OE, Dash JG, Sing B, Wettlaufer JS. 2000. Frost heave in argon. *Phys. Rev. Lett.* 85:4908–11

Zhu Y, Granick S. 2003. Reassessment of solidification in fluids confined between mica sheets. *Langmuir* 19:8148–51

Contents

INDEXES

ERRATA

An online log of corrections to *Annual Review of Fluid Mechanics*
chapters may be found at http://fluid.annualreviews.org/errata.shtml